Editors' Suggestion

Dynamic Control of the Coupling between Dark and Bright Excitons with Vibrational Strain

Ryuichi Ohta, Hajime Okamoto, Takehiko Tawara, Hideki Gotoh, and Hiroshi Yamaguchi
NTT Basic Research Laboratories, NTT Corporation, 3-1 Morinosato Wakamiya, Atsugi-shi, Kanagawa 243-0198, Japan

(Received 3 April 2018; published 26 June 2018)

We numerically and experimentally investigate strain-induced coupling between dark and bright excitons and its dynamic control using a gallium arsenide (GaAs) micromechanical resonator. Uniaxial strain induced by the mechanical resonance efficiently detunes the exciton energies and modulates the coupling strength via the deformation potential in GaAs. This allows optical access to the long-lived dark states without using any external electromagnetic field. This field-free approach could be expanded to a wide range of solid-state materials, leading to on-chip excitonic memories and circuits based on micromechanical resonators.

DOI: 10.1103/PhysRevLett.120.267401

In many physical systems, there are specific electronic states called "dark states" [1–4] that are protected from rapid radiative decay to conserve the system's angular momentum. Generally, the optical transition in solid-state systems obeys the selection rule on the spin configuration of electrons and holes. For instance, in the III-V semiconductor gallium arsenide (GaAs), electrons in the conduction band and holes in the heavy-hole band with antiparallel spins are optically active and are called bright excitons, and those with parallel spins are optically inactive and are called dark excitons. Such dark excitons are of great interest owing to their long-lived nature, indicating their potential for quantum information [1,2,5,6] and spintronic applications [7]. However, their high stability comes at the expense of optical inaccessibility, which limits the practical usage of the dark states. A magnetic [8–10] or electric [7,11] field has been used to break the symmetry of the crystal field and to allow optical access to the dark excitons. Alternatively, optically accessible intermediate states [12], surface plasmon polaritons [13], magnetic impurities [14], and a cleaved facet [15] have been utilized to access the long-lived dark states.

In this Letter, we numerically and experimentally investigate a new scheme to optically access the dark excitons using a time-varying strain in a micromechanical resonator. The uniaxial strain induced by the mechanical motion of the GaAs cantilever breaks the symmetry of the crystal field and mixes dark and bright excitons via the deformation potential [16]. Therefore, the mechanical oscillation allows the dark exciton to be optically accessible. We clearly observed avoided crossings of dark and bright exciton states induced by the mechanical oscillation, which is evidence of the coupling between the two states. In contrast to the reported schemes, our approach does not require any external electromagnetic fields. This is advantageous in its manipulation and will enable us to extend this scheme to the other solid-state materials, including one- [17–20] and two-dimensional [10,21–23] materials. Unlike the magnetic schemes, this approach would allow high-speed operation, for instance, gigahertz access to the dark states with high-frequency acoustic devices [24–26]. These advantages are preferable to manipulate dark states in solid-state platforms and will open the way towards the development of on-chip memories and logics based on micromechanical resonators.

For the zinc-blende structure such as GaAs, strain effects in the bound exciton states are theoretically described by the Pikus-Bir Hamiltonian [27,28] in the $\boldsymbol{k}\cdot\boldsymbol{p}$ model as follows:

$$\begin{pmatrix} P_\epsilon+Q_\epsilon & L_\epsilon & M_\epsilon & 0 \\ L_\epsilon^* & P_\epsilon-Q_\epsilon & 0 & M_\epsilon \\ M_\epsilon^* & 0 & P_\epsilon-Q_\epsilon-\varepsilon_{\mathrm{ex}} & -L_\epsilon \\ 0 & M_\epsilon^* & -L_\epsilon^* & P_\epsilon+Q_\epsilon-\varepsilon_{\mathrm{ex}} \end{pmatrix} \begin{pmatrix} |\mathrm{BX_{HH}}\rangle \\ |\mathrm{BX_{LH}}\rangle \\ |\mathrm{DX_{LH}}\rangle \\ |\mathrm{DX_{HH}}\rangle \end{pmatrix}, \tag{1a}$$

$$P_{\epsilon(t)} = (a_c - a_v)(\epsilon_{xx}+\epsilon_{yy}+\epsilon_{zz}), \tag{1b}$$

$$Q_{\epsilon(t)} = -b(\epsilon_{xx}+\epsilon_{yy}-2\epsilon_{zz})/2, \tag{1c}$$

$$L_{\epsilon(t)} = d(\epsilon_{xz} - i\epsilon_{yz}), \tag{1d}$$

$$M_{\epsilon(t)} = \sqrt{3}b(\epsilon_{xx} - \epsilon_{yy})/2, \tag{1e}$$

where BX (DX) stands for bright (dark) excitons and the subscript of HH (LH) specifies a heavy-hole (light-hole) band. P_ϵ, Q_ϵ, L_ϵ, and M_ϵ are derived from strain tensors (ϵ_{ij}) and the deformation potentials of GaAs (a_c, a_v, b, d) [27,28]. $\varepsilon_{\mathrm{ex}}$ is the exchange energy of an electron and a hole [29]. The off-diagonal components M_ϵ cause interband mixings, allowing the hybridization of different total angular momentum states, i.e., bright excitons and dark excitons. Such strain-induced coupling has been demonstrated using epitaxial strain in III-V semiconductor heterostructures and quantum dots [16]. However, the epitaxial strain cannot be controlled after the sample preparation. Its isotropic strain distribution ($\epsilon_{xx} \approx \epsilon_{yy}$), moreover, is not suitable for achieving sufficient coupling.

Acoustic devices, such as piezoelectric actuators [30] and interdigital transducers [17], induce dynamic strain and have so far externally controlled exciton properties via deformation potentials. Here, we use a micromechanical resonator composed of an n-doped $Al_{0.3}Ga_{0.7}As$, an undoped GaAs, and an undoped superlattice of $Al_{0.3}Ga_{0.7}As$ and GaAs as shown in Fig. 1(a), in which exciton states are modulated at the resonance frequency of the mechanical mode. In contrast to the other acoustic devices, the mechanical resonator significantly amplifies the amount of the vibrational strain by its high-quality factor. Local strain distribution (ϵ_{ij}) in the resonator can be tailored by the mode shape; for instance, anisotropic strain ($\epsilon_{xx} \neq \epsilon_{yy}$) is generated by flexural modes. Thus, we can dynamically induce a large enough strain to couple the dark and bright excitons with the external driving via a piezoelectric actuator.

Figure 1(b) shows the calculated energies of the bright and dark excitons in the mechanical resonator with respect to the mechanical displacements, where the strain tensors are calculated with the finite element method (FEM) (see Supplemental Material [31]). We took account of the contribution from the intrinsic isotropic strain caused by the epitaxial mismatch, which splits the exciton energies of the HH and LH bands when the cantilever is in the equilibrium position [32]. The uniaxial strain induced by the mechanical motion causes additional energy splits and mixing of the bright excitons in the LH band and the dark excitons in the HH band, which can be seen when the mechanical displacement reaches 15 nm [Fig. 1(b)].

Figure 1(c) shows the experimental setup used in this study. It consists of a Ti:sapphire (Ti:Sa) pump laser, charge coupled device (CCD), and Doppler interferometer. The exciton energies were characterized with a photoluminescence (PL) measurement, while the mechanical displacement was simultaneously measured with the interferometer. The sample preparation and the experimental setup are described in the Supplemental Material [31]. Figure 2(a) shows a typical PL spectrum obtained at the midpoint of the resonator. The position dependence of the PL spectra is discussed in the Supplemental Material [31]. The three higher (lower) energy peaks are attributed to

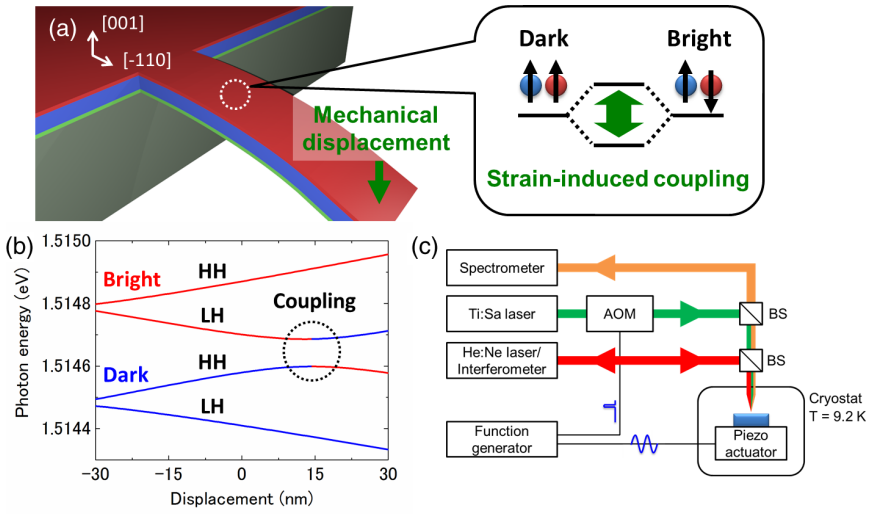

FIG. 1. (a) Schematic image of the mechanical resonator and strain-induced coupling of dark and bright excitons. Uniaxial in-plane strain hybridizes different total angular momentum states. (b) Energy diagram of dark and bright bound excitons with mechanical displacement calculated from Eq. (1). In-plane strain modulates the splitting of heavy-hole (HH) and light-hole (LH) bands and generates coupling between dark and bright excitons. (c) Experimental setup for characterizing the optical and mechanical properties of a resonator with bound excitons. PL spectra were obtained with a 780-nm Ti:Sa pump laser. Mechanical motion was measured using a Doppler interferometer with a 633-nm He:Ne laser. The resonator was placed on a piezoactuator to drive it at the resonance frequency. Experiments were performed in a vacuum (2×10^{-5} Pa) at 9.2 K.

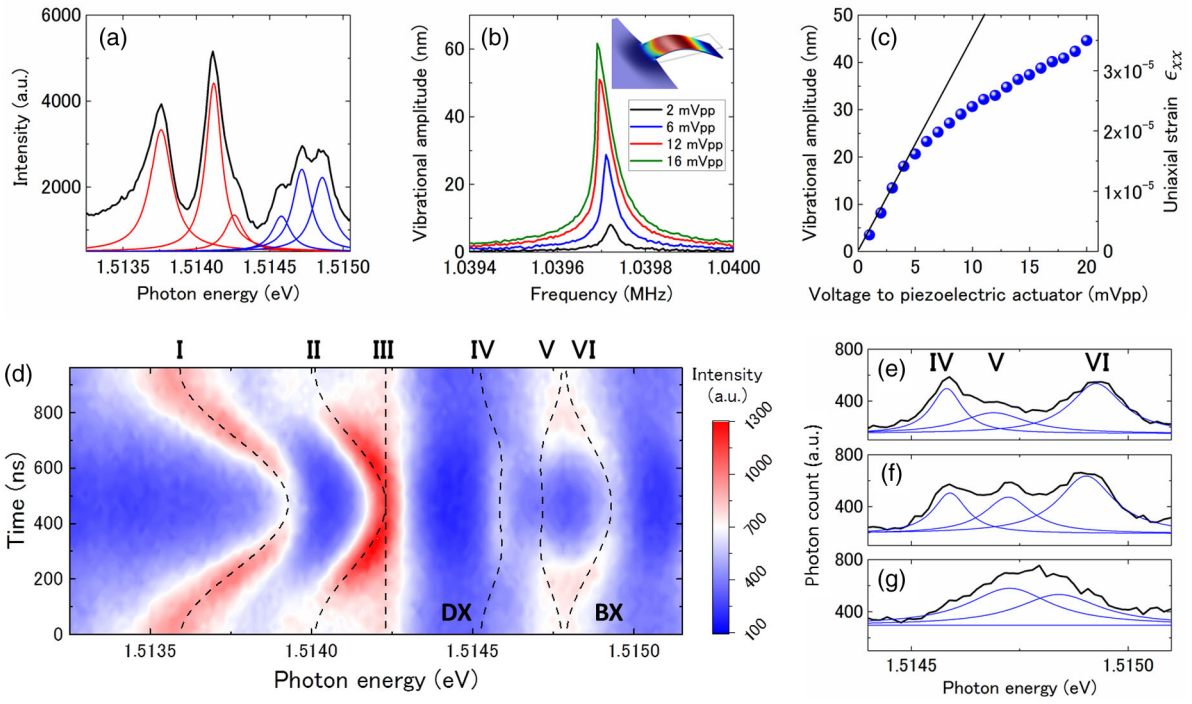

FIG. 2. (a) PL spectrum obtained at the midpoint of the resonator. It is fitted by Lorenz functions. Red (blue) peaks are attributed to acceptor (donor) bound excitons. (b) Frequency response of the second flexural mode of the resonator excited by the piezoactuator. (Inset) The strain distribution calculated by the FEM. (c) Voltage dependence of the vibrational amplitude and the corresponding in-plane strain of the resonator at the resonance frequency. Solid line fits the voltage dependence in the linear regime. (d) Wide-range stroboscopic PL spectrum. Peaks I–III (IV–VI) are attributed to acceptor (donor) bound excitons. The dashed lines indicate their peak energies. DX and BX represent dark and bright exciton energies. (e)–(g) Cross-sectional PL spectra of donor bound excitons at 480 (e), 320 (f), and 0 ns (g). Peaks IV and V show avoided crossing at 320 and 640 ns, respectively, indicating the coherent coupling of the two states. Peak IV is attributed to the dark exciton, which is optically inactive when it is detuned from peak V.

donor (acceptor) bound excitons [33]. To induce time-varying strain at that midpoint, the second-order flexural mode with 1.04 MHz was electrically excited by a piezoactuator. Figure 2(b) shows the frequency response of this mechanical mode at various drive voltages, where the inset shows the strain distribution calculated by the FEM. A mechanical Q of 30 000 is extracted from the linewidth. The vibrational amplitude at the resonance frequency and the corresponding uniaxial strain are shown in Fig. 2(c). The mechanical nonlinearity gradually saturates the vibrational amplitude when the actuation voltage exceeds 5 mV_{pp}, while the corresponding strain is high enough to cause the coupling as estimated from Fig. 1(b).

We employed stroboscopic PL measurements [17–19] to investigate the effects of mechanically induced strain on the bound exciton energies. The pump laser was shaped into a periodic rectangular pulse with an acousto-optical modulator (AOM), whose repetition rate was synchronized to the mechanical frequency. By changing the relative phase between the pump pulse and the mechanical motion, PL spectra under time-varying strain were obtained with a CCD. Figure 2(d) shows stroboscopic PL spectra of bound exciton states for a drive voltage of 12 mV_{pp}. Figures 2(e)–2(g) are cross-sectional PL spectra of donor bound excitons at 480, 320, and 0 ns, respectively. Each spectrum is fitted by a Lorentz function with the peaks labeled I to VI, and their peak energies are traced as dashed lines in Fig. 2(d). The vibrational strain sinusoidally modulates peaks I and II, whereas peak III is less affected. These behaviors reproduce the energy shifts of acceptor bound excitons characterized by static strain experiments [34,35]. The sinusoidal energy shifts indicate that the bound excitons are localized at the one side of the heterojunction, so that the strain intensity for each bound exciton is almost same, although the strain field continuously varies along the vertical direction. Mechanical bending additionally modulates the PL intensity via the piezoelectric effect [36], which is proportional to the magnitude of the in-plane strain. The piezoelectric effect causes a potential gradient and modifies carrier distributions. It reduces the PL intensities around 480 ns. Although the electric field affects the exciton spins via spin-orbit interaction, the field intensity owing to the piezoelectric effect is too small to mix them. The vibrational strain also modulates the energy difference of peaks V and VI, which originate from the bright exciton states bound by donors. The most interesting feature can be seen around 320 and 640 ns, where peak V shows avoided crossing with peak IV.

Peak IV is attributed to dark excitons in accordance with Ref. [29]. In fact, its PL intensity vanishes when the energy is detuned from peak V. The avoided crossing is a clear sign that the bright and dark excitons are coupled by mechanically induced strain.

To investigate the mechanically hybridized exciton states quantitatively, we numerically calculated the energies and PL spectra of bound excitons with the Pikus-Bir Hamiltonian in the $\boldsymbol{k}\cdot\boldsymbol{p}$ model. We derived the values of P_ϵ, Q_ϵ, L_ϵ, and M_ϵ from the measured mechanical amplitudes and the calculated strain tensors with the FEM. Figures 3(a)–3(d) show the measured PL spectra and calculated dark and bright bound exciton energies (dashed lines) at drive voltages of 2, 6, 12, and 16 mV_{pp}. Figures 3(e)–3(h) show the calculated PL spectra, where the linewidths of the dark and bright excitons (γ_D, γ_B) are 70 μeV (see Supplemental Material [31]). The good agreement between the experiments and the theoretical analysis verifies the hybridization of the dark and bright bound excitons via mechanical oscillation. The coupling strength (g_DB) is estimated to be about 50 μeV, which is on the same order as the linewidths.

The $\boldsymbol{k}\cdot\boldsymbol{p}$ model analysis indicates that g_DB can be further improved by tailoring the strain distribution, i.e., the magnitude and anisotropy of the strain tensors. To enhance g_DB, we should maximize M_ϵ and inject a large vibrational amplitude. However, large vibrational amplitudes cause the energy detuning of dark and bright excitons. So, we should simultaneously minimize P_ϵ and Q_ϵ to involve the strong interaction in the two states. A large M_ϵ and a small P_ϵ and Q_ϵ are generated by the anisotropic strain

$$\epsilon_{xx} = -\epsilon_{yy}, \qquad \epsilon_{zz} = 0,$$

which results in the following diagonal and off-diagonal terms

$$M_\epsilon = \sqrt{3}b\epsilon_{xx}, \qquad P_\epsilon = Q_\epsilon = 0.$$

Such anisotropic strain can be realized in a drum-shaped resonator as shown in Figs. 4(a) and 4(b), whereas a cantilever dominantly causes the uniaxial strain. Here, we consider two orthogonal modes, mode H and mode V, and focus their cross point where $\epsilon_{xx} = -\epsilon_{yy}$ and $\epsilon_{zz} = 0$. Figures 4(c)–4(h) show ϵ_{xx}, ϵ_{yy}, and ϵ_{zz} in mode H and mode V calculated by the FEM. We calculated the PL spectrum from dark and bright excitons with the experimentally available vibrational amplitude (0–20 nm) as shown in Fig. 4(i). g_DB reaches 1 meV, which is much larger than the exciton linewidths (γ_B, γ_D) obtained in this experiments. The cooperativity ($C = 4{g_\mathrm{DB}}^2/\gamma_\mathrm{B}\gamma_\mathrm{D}$) exceeds 800 and thus allows the coherent manipulation of dark and bright bound exciton states.

Moreover, the Pikus-Bir Hamiltonian suggests that the off-diagonal terms of L_ϵ, namely, the shear strain of ϵ_{xz} and ϵ_{yz}, cause additional coupling between $|\mathrm{BX_{HH}}\rangle$ and $|\mathrm{BX_{LH}}\rangle$ (g_BB) and $|\mathrm{DX_{LH}}\rangle$ and $|\mathrm{DX_{HH}}\rangle$ (g_DD). The shear strain is generated by torsional oscillation and is concentrated near the side edges of the resonator. We evaluated the additional exciton-exciton couplings in the second-order torsional mode of this cantilever shown in Fig. 4(j). Figure 4(k) shows the calculated population of each bound exciton state at the circled position in Fig. 4(j), which describes the three

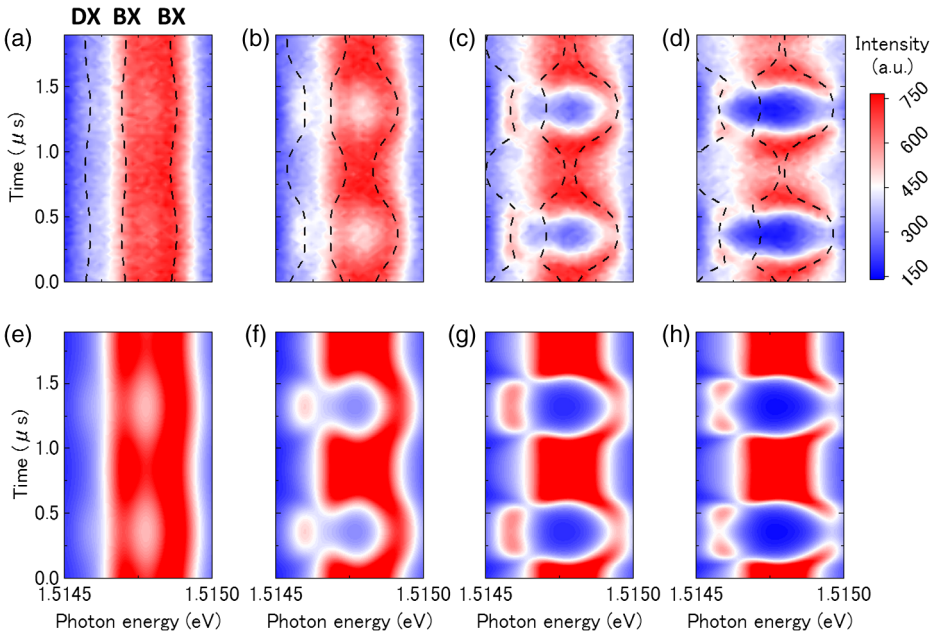

FIG. 3. (a)–(d) Stroboscopic PL spectra obtained with drive voltages of (a) 2, (b) 6, (c) 12, and (d) 16 mV_{pp}. The dashed lines are the eigenenergies of bound excitons calculated from Eq. (1) with measured parameters. (e)–(h) Numerically calculated PL spectra at the corresponding vibrational amplitudes of (a)–(d).

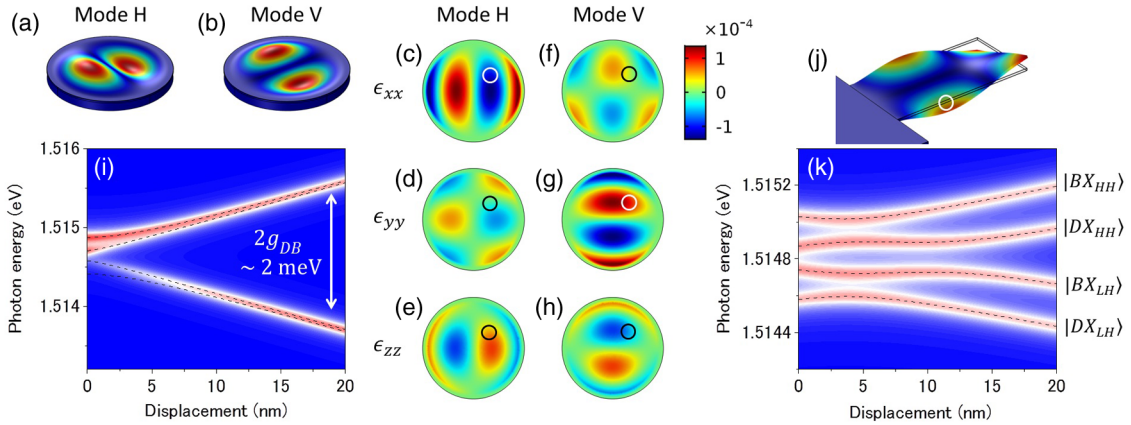

FIG. 4. (a)–(b) Mechanical amplitudes of horizontal (a) and vertical (b) modes in a drum-shaped resonator. The radius and thickness are 20 μm and 600 nm. (c)–(h) Spatial distribution of ϵ_{xx} (c),(f), ϵ_{yy} (d),(g), and ϵ_{zz} (e),(h) in mode H (c)–(e) and mode V (f)–(h) at the vibration amplitude of 10 nm. (i) Calculated PL spectra from dark and bright bound excitons with the strain tensors at the circled position in (c)–(h). It shows the strong coupling with a g_{DB} of 1 meV, where the detuning of the dark and bright excitons is not significantly changed by mechanical displacement. (j) The second-order torsional mechanical mode in the cantilever calculated with the FEM. (k) Displacement dependence of the dark and bright bound exciton states calculated from Eq. (1) with the parameters from experiments. L_ϵ causes the coupling of $|\mathrm{BX_{HH}}\rangle$ and $|\mathrm{BX_{LH}}\rangle$ and $|\mathrm{DX_{LH}}\rangle$ and $|\mathrm{DX_{HH}}\rangle$ at 4 nm, while M_ϵ provides the coupling of $|\mathrm{DX_{HH}}\rangle$ and $|\mathrm{BX_{LH}}\rangle$ at 10 nm.

avoided crossings, representing the coherent couplings in multiple dark and bright excitons (see Supplemental Material [31]).

In conclusion, we demonstrated dynamic control of the strain-induced coupling between dark and bright bound excitons and the optical accessibility to the dark state using a mechanical resonator. Good agreements between the experimental results and numerical calculations from the $\boldsymbol{k}\cdot\boldsymbol{p}$ model indicate that the vibrational strain causes the hybridization of the two states. The coupling strength (g_{DB}, g_{BB}, and g_{DD}) could be further improved by tailoring the strain distribution. This mechanical approach would be widely applied to any solid-state two-level system, such as quantum dots [18,19,37,38] and nitrogen-vacancy centers [39,40], and make it possible to realize on-chip excitonic memories and circuits.

We thank Y. Matsuzaki, M. Asano, S. Houri, K. Takata, and S. Adachi for discussions about the theoretical models and fruitful comments on the manuscript. This Letter is partly supported by MEXT KAKENHI Grant No. (JP15H05869 and JP16H01057).

[1] M. Fleischhauer and M. D. Lukin, Phys. Rev. Lett. **84**, 5094 (2000).
[2] X. Xu, B. Sun, P. R. Berman, D. G. Steel, A. S. Bracker, D. Gammon, and L. J. Sham, Nat. Phys. **4**, 692 (2008).
[3] M. Nirmal, D. J. Norris, M. Kuno, M. G. Bawendi, Al. L. Efros, and M. Rosen, Phys. Rev. Lett. **75**, 3728 (1995).
[4] Z. Zhu, Y. Matsuzaki, R. Amsuss, K. Kakuyanagi, T. Shimo-Oka, N. Mizuochi, K. Nemoto, K. Semba, W. J. Munro, and S. Saito, Nat. Commun. **5**, 3424 (2014).
[5] A. Nazarkin, R. Netz, and R. Sauerbrey, Phys. Rev. Lett. **92**, 043002 (2004).
[6] T. Chanelière, D. N. Matukevich, S. D. Jenkins, S.-Y. Lan, T. A. B. Kennedy, and A. Kuzmich, Nature (London) **438**, 833 (2005).
[7] J. McFarlane, P. A. Dalgarno, B. D. Gerardot, R. H. Hadfield, R. J. Warburton, K. Karrai, A. Badolato, and P. M. Petroff, Appl. Phys. Lett. **94**, 093113 (2009).
[8] Al. L. Efros, M. Rosen, M. Kuno, M. Nirmal, D. J. Norris, and M. Bawendi, Phys. Rev. B **54**, 4843 (1996).
[9] M. Bayer, O. Stern, A. Kuther, and A. Forchel, Phys. Rev. B **61**, 7273 (2000).
[10] X.-X. Zhang *et al.*, Nat. Nanotechnol. **12**, 883 (2017).
[11] R. M. Kraus, P. G. Lagoudakis, A. L. Rogach, D. V. Talapin, H. Weller, J. M. Lupton, and J. Feldmann, Phys. Rev. Lett. **98**, 017401 (2007).
[12] E. Poem, Y. Kodriano, C. Tradonsky, N. H. Lindner, B. D. Gerardot, P. M. Petroff, and D. Gershoni, Nat. Phys. **6**, 993 (2010).
[13] Y. Zhou *et al.* Nat. Nanotechnol. **12**, 856 (2017).
[14] M. Goryca, P. Plochocka, T. Kazimierczuk, P. Wojnar, G. Karczewski, J. A. Gaj, M. Potemski, and P. Kossacki, Phys. Rev. B **82**, 165323 (2010).
[15] Y. H. Huo, V. Křápek, O. G. Schmidt, and A. Rastelli, Phys. Rev. B **95**, 165304 (2017).
[16] I. Schwartz, E. R. Schmidgall, L. Gantz, D. Cogan, E. Bordo, Y. Don, M. Zielinski, and D. Gershoni, Phys. Rev. X **5**, 011009 (2015).
[17] M. Weiß *et al.*, Nano Lett. **14**, 2256 (2014).
[18] I. Yeo *et al.*, Nat. Nanotechnol. **9**, 106 (2014).
[19] M. Montinaro, G. Wüst, M. Munsch, Y. Fontana, E. Russo-Averchi, M. Heiss, A. Fontcuberta i Morral, R. J. Warburton, and M. Poggio, Nano Lett. **14**, 4454 (2014).
[20] M. Munsch, A. V. Kuhlmann, D. Cadeddu, J.-M. Gérard, J. Claudon, M. Poggio, and R. J. Warburton, Nat. Commun. **8**, 76 (2017).

[21] J. P. Mathew, R. N. Patel, A. Borah, R. Vijay, and M. M. Deshmukh, Nat. Nanotechnol. **11**, 747 (2016).
[22] M. Will, M. Hamer, M. Müller, A. Noury, P. Weber, A. Bachtold, R. V. Gorbachev, C. Stampfer, and J. Güttinger, Nano Lett. **17**, 5950 (2017).
[23] Z. Ye, T. Cao, K. O'Brien, H. Zhu, X. Yin, Y. Wang, S. G. Louie, and X. Zhang, Nature (London) **513**, 214 (2014).
[24] E. A. Laird, F. P. W. Tang, G. A. Steele, and L. P. Kouwenhoven, Nano Lett. **12**, 193 (2012).
[25] K. C. Balram, M. I. Davanco, J. D. Song, and K. Srinivasan, Nat. Photonics **10**, 346 (2016).
[26] X. L. Feng, C. J. White, A. Hajimiri, and M. L. Roukes, Nat. Nanotechnol. **3**, 342 (2008).
[27] T. B. Bahder, Phys. Rev. B **41**, 11992 (1990).
[28] O. Stier, M. Grundmann, and D. Bimberg, Phys. Rev. B **59**, 5688 (1999).
[29] Y. Abe, J. Phys. Soc. Jpn. **19**, 818 (1964).
[30] J. Zhang, J. S. Wildmann, F. Ding, R. Trotta, Y. Huo, E. Zallo, D. Huber, A. Rastelli, and O. G. Schmidt, Nat. Commun. **6**, 10067 (2015).
[31] See Supplemental Material at http://link.aps.org/supplemental/10.1103/PhysRevLett.120.267401 for details on the $\boldsymbol{k}\cdot\boldsymbol{p}$ models (Sec. 1–2, 5), descriptions of the sample preparation and experimental setup (Sec. 3), a discussion on the position dependence of PL spectra (Sec. 4).
[32] Y. H. Huo *et al.*, Nat. Phys. **10**, 46 (2014).
[33] D. G. Allen, M. S. Sherwin, and C. R. Stanley, Phys. Rev. B **72**, 035302 (2005).
[34] M. Schmidt, T. N. Morgan, and W. Schairer, Phys. Rev. B **11**, 5002 (1975).
[35] V. A. Karasyuk, M. L. W. Thewalt, and A. J. Springthorpe, Phys. Status Solidi (b) **210**, 353 (1998).
[36] T. Sogawa, H. Sanada, H. Gotoh, H. Yamaguchi, and P. V. Santos, Appl. Phys. Lett. **100**, 162109 (2012).
[37] I. Wilson-Rae, P. Zoller, and A. Imamoglu, Phys. Rev. Lett. **92**, 075507 (2004).
[38] T. Nakaoka, T. Kakitsuka, T. Saito, S. Kako, S. Ishida, M. Nishioka, Y. Yoshikuni, and Y. Arakawa, J. Appl. Phys. **94**, 6812 (2003).
[39] A. Barfuss, J. Teissier, E. Neu, A. Nunnenkamp, and P. Maletinsky, Nat. Phys. **11**, 820 (2015).
[40] P. Ovartchaiyapong, K. W. Lee, B. A. Myers, and A. C. B. Jayich, Nat. Commun. **5**, 4429 (2014).